RESEARCH ARTICLE

# The Role of Lipoprotein-Associated Phospholipase A₂ in a Murine Model of Experimental Autoimmune Uveoretinitis

G. L. Crawford[1], J. Boldison[2], D. A. Copland[1], P. Adamson[3], D. Gale[4], M. Brandt[5], L. B. Nicholson[1,2], A. D. Dick[1,2]*

1 Academic unit of Ophthalmology, School of Clinical Sciences, University of Bristol, Bristol, United Kingdom, 2 School of Cellular and Molecular Medicine, University of Bristol, Bristol, United Kingdom, 3 Ophthiris Discovery Performance Unit, GlaxoSmithKline, Stevenage, United Kingdom, 4 Ophthiris Discovery Performance Unit, GlaxoSmithKline, King of Prussia, Pennsylvania, United States of America, 5 Platform Technology Sciences, King of Prussia, Pennsylvania, United States of America

* a.dick@bristol.ac.uk

## Abstract

Macrophage activation is, in part, regulated via hydrolysis of oxidised low density lipoproteins by Lipoprotein-Associated phospholipase A₂ (Lp-PLA₂), resulting in increased macrophage migration, pro-inflammatory cytokine release and chemokine expression. In uveitis, tissue damage is mediated as a result of macrophage activation; hence inhibition of Lp-PLA₂ may limit macrophage activation and protect the tissue. Utilising Lp-PLA₂ gene-deficient (KO) mice and a pharmacological inhibitor of Lp-PLA (SB-435495) we aimed to determine the effect of Lp-PLA₂ suppression in mediating retinal protection in a model of autoimmune retinal inflammation, experimental autoimmune uveoretinitis (EAU). Following immunisation with RBP-3 (IRBP) 1–20 or 161–180 peptides, clinical disease was monitored and severity assessed, infiltrating leukocytes were enumerated by flow cytometry and tissue destruction quantified by histology. Despite ablation of Lp-PLA₂ enzyme activity in Lp-PLA₂ KO mice or wild-type mice treated with SB-435495, the number of infiltrating CD45⁺ cells in the retina was equivalent to control EAU animals, and there was no reduction in disease severity. Thus, despite the reported beneficial effects of therapeutic Lp-PLA₂ depletion in a variety of vascular inflammatory conditions, we were unable to attenuate disease, show delayed disease onset or prevent progression of EAU in Lp-PLA₂ KO mice. Although EAU exhibits inflammatory vasculopathy there is no overt defect in lipid metabolism and given the lack of effect following Lp-PLA₂ suppression, these data support the hypothesis that sub-acute autoimmune inflammatory disease progresses independently of Lp-PLA₂ activity.

## Introduction

Non-anterior uveitis (posterior, pan and intermediate uveitis) is a collective term used to describe a range of intraocular inflammatory disorders affecting the uvea and retina, and whilst more rare than anterior uveitis, is significantly more sight threatening [1]. Uveitis accounts for 10% of the 285 million visually impaired patients worldwide [2] with considerable financial and social implications, as it predominantly effects the working age population [3]. Uveitis is presumed autoimmune or immune mediated when infectious aetiology has been excluded [1, 4–6]. In mice, experimental autoimmune uveoretinitis (EAU) is an antigen-specific Th1/Th17 CD4$^+$ T cell-directed murine model, employed to mimic human non-infectious, non-anterior uveitis, which has been utilised extensively to develop a detailed understanding of the immuno-pathogenesis of vascular inflammation, retinal leukocyte infiltration and mechanisms of tissue damage [6–8]. In this model, tissue destruction is dependent upon activation and infiltration of mononuclear cell infiltration [6, 9–12].

Tissue inflammation is held in check and homeostasis maintained, in part through microglia (resident retinal myeloid cell population) but following breakdown of blood ocular barrier [13] circulating macrophages infiltrate the retina early in the course of EAU [7, 14]. The migration of CD4$^+$ T cells to the retina causes activation and further accumulation of CD11b$^+$ macrophages. Macrophages display broad heterogeneity and their phenotype and behaviour is regulated by a plethora of stimuli found in the local microenvironment. For example, macrophages can inhibit T-cell proliferation in the eye but also produce tissue-damaging superoxides [7, 15, 16]. Notwithstanding, regulating macrophage activation will reduce inflammation [17, 18] and as such, an ability to manipulate macrophage phenotype and/or migration has the potential to abrogate EAU onset.

One means of repressing macrophage activation is through prevention of hydrolysis of oxidised low density lipoproteins (oxLDL), catalysed by the enzyme Lipoprotein Associated Phospholipase A₂ (Lp-PLA₂). This reaction produces lysophosphatidylcholine (LPC) and oxidised non-esterified fatty acids (ox-NEFA) two potent pro-inflammatory mediators, which up-regulate expression of chemokines and adhesion molecules, induce macrophage migration and promote pro-inflammatory cytokine release [19, 20]. The phospholipase A₂ (PLA₂) family are a group of enzymes involved in catalysing the hydrolysis of fatty acyl moieties from the sn-2 position of oxidized phospholipid molecules [19]. Lp-PLA₂ is a 45kDa secreted enzyme, expressed by monocytes, macrophages, T cells and mast cells. This enzyme contains a catalytic serine residue [21] and is active in basal physiological conditions. Unlike other PLA₂ family members, Lp-PLA₂ functions independently of calcium and is highly specific for substrates with a short chain fatty acyl residue at the sn-2 position, meaning it does not hydrolyse membrane phospholipids [22].

Lp-PLA₂ suppression has been used to modulate disease in both atherosclerosis and diabetic macular oedema models [23], which in common with uveitis, present with macrophage mediated tissue damage and underlying vascular pathology. It was first noted that Lp-PLA₂ expression was high in atherosclerotic plaques, particularly those which were necrotic and prone to rupture and a meta-analysis of nearly 80,000 people demonstrated a continuous association between the mass and activity of Lp-PLA₂ and risk of coronary heart disease [24]. A diabetic and hypercholesterolemic swine model was used to test the efficacy of Lp-PLA₂ depletion in atherosclerosis. In short, treatment of atherosclerotic pigs with Darapladib, a selective, reversible inhibitor of Lp-PLA₂ [25] induced a significant reduction in lesion development and necrotic core area [26]. Similar results were also noted in the human Integrated Biomarker and Imaging Study 2 (IBIS-2) [27] whereby ultrasound analysis confirmed that Darapladib treated patients had smaller coronary artery lesions than those receiving a placebo control. Furthermore,

Darapladib has been shown to attenuate expression of monocyte chemoattractant protein 1 (MCP-1), VCAM-1 and TNF-$\alpha$ gene expression, [28] and demonstrate reduced cerebral vascular permeability in the diabetic/hypercholesterolemic swine model [23]. These data further implicate Lp-PLA$_2$ inhibition as a promising therapeutic target for prevention or resolution of inflammation and vascular permeability.

In light of success in other models of macrophage mediated vascular inflammatory pathologies, albeit not in autoimmune disease, and given that tissue damage in uveitis is dependent upon macrophage infiltration and activation, we utilised Lp-PLA$_2$ knockout (KO) mice and a specific Lp-PLA$_2$ pharmacological inhibitor SB-435495 (referred to herein as Lp-PLA$_2$ *deletion* or *inhibition* respectively) to determine the role of Lp-PLA$_2$ in autoimmune retinal inflammation. The prediction being that enzyme depletion would suppress macrophage activation in the face of a T cell driven disease. However, despite the reported beneficial effects of therapeutic Lp-PLA$_2$ depletion in a variety of vascular inflammatory conditions, in the murine EAU model, suppression of Lp-PLA$_2$ activity was unable to attenuate disease or show delayed disease onset.

## Methods

### Mice

C57BL/6 Lp-PLA$_2$ knockout mice (-/-, KO), and heterozygous (-/+, HET) and WT littermate controls were obtained from GlaxoSmithKline (Philadelphia, USA and Stevenage, UK). The Lp-PLA$_2$ KO animals were generated by GlaxoSmithKline using 129/BL6 ES cells. Single nucleotide polymorphism (SNP) analysis was used throughout breeding to generate animals that were >98% C57BL/6. The colony was then established in the UK and SNP analysis was re-run to confirm the genetic background of the mice (>99% C57BL/6) [29]. The animals have no physical or immunological phenotype. B10 RIII mice are inbred colonies at University of Bristol Animal Services Unit. All mice were housed in specific pathogen free conditions with continual access to food and water. Female mice aged 6–8 weeks were immunised for EAU, and housed according to Home Office regulations in the University of Bristol animal house facility. Treatment of animals was carried out in accordance with the European Directive 86/609/EEC, the GlaxoSmithKline Policy on the Care, Welfare and Treatment of Animals and conformed to the Association for Research in Vision and Ophthalmology animal policy (ARVO statement for the use of Animals in Ophthalmic and Vision Research). Mice were sacrificed by recognised schedule one methods and all animal work was approved by the University of Bristol ethical approval group.

### Reagents

Human RBP-3$_{161-180}$ (SGIPYIISYLHPGNTILHVD) and RBP-3$_{1-20}$ peptide (GPTHLFQPSLVLDMAKVLLD) were synthesised by Sigma-Aldrich (Poole, U.K) and Severn Biotech (Worcester, U.K) respectively. High performance liquid chromatography was used to confirm peptide purity of >95%, and aliquots of peptide preparations were stored at -80°C. SB-435495 and vehicle solution were provided by GlaxoSmithKline (Stevenage, UK). Complete media comprising Dulbecco's modified Eagle medium (DMEM) supplemented with 10% heat inactivated foetal calf serum (FCS), 100U/ml penicillin-streptomycin, 2mmol/L L-Glutamine and Sodium pyruvate (Invitrogen, Paisley, U.K).

## EAU induction and treatment

C57BL/6 and B10RIII mice were immunised subcutaneously (s.c) in one flank with 50μg RBP-3 $_{1-20}$ or 50μg RBP-3 $_{161-180}$ respectively. Peptides were prepared in water (2% DMSO), emulsified in CFA (1mg/ml 1:1 v/v) and supplemented with 1.5mg.ml *Mycobacterium tuberculosis* complete H37 Ra (BD Biosciences, Oxford, U.K.). A simultaneous I.P injection of 1.5μg *Bordella pertussis* toxin (Tocris, Bristol, UK) was also administered. Doses of SB-435495, phosphate buffered saline (PBS) or vehicle solution were administered by I.P injection once or twice daily (9am or 9am/pm respectively) as described (S4 Fig).

## EAU clinical assessment

Digital images of the retina were obtained by topical endoscopic fundus imaging (TEFI) using a protocol described previously by Paques *et al* [30] and subsequently validated for EAU [8]. In short, a Nikon D80 digital camera, with a 10-million pixel charge-coupled device image sensor and Nikkor AF 85 /F1.8 D objective and additional +4.00 dioptre magnifying lens, (Nikon, Tokyo, Japan), 5cm long, 3mm diameter teleotoscope (1218AA: Karl Storz, Tuttlington, Germany), and xenon lamp were used to capture colour images of the retinal fundus. Topical application of phenylephrine 2.5% and tropicamide 1% (Minims; Chauvin Pharmaceuticals, Romford,UK), was used to dilate the pupil, while corneal anaesthesia was achieved by topical application of oxybuprocaine 0.4% (Minims). Viscous eye gel (Novartis Pharmaceuticals, Camberley, UK) allowed digital images to be obtained by direct corneal contact with the endoscope. All images were cropped using Photoshop CS software (Adobe, Mountain view, California, USA). Using an adapted clinical grading system, fundal images were scored according to inflammatory changes to the optic disc and retinal vessels in addition to retinal lesions and structural damage [31].

## Sample collection and cell preparation

Blood samples were obtained via cardiac puncture, collected in neonatal KE/1.3 1.3ml EDTA tubes and centrifuged for 8 minutes at 1800rpm and 4°C. The plasma fraction was removed and stored at -80°C for plasma Lp-PLA₂ enzyme activity and plasma SB-435495 analysis (GlaxoSmithKline). The enucleated right eye was placed in sterile DMEM for retinal dissection and flow cytometric analysis, the left eye was orientated in optimal cutting temperature (OCT) compound and snap frozen in liquid nitrogen for histology. Spleens were also removed for flow cytometry and histology.

Spleen and thymus were mashed and filtered through a 40μm cell strainer to remove cellular debris. Splenocytes were re-suspended in 1ml ACK salt solution (Ammonium-chloride-potassium lysing buffer, 8,024mg/L $NH_4CL$, 1,001mg/L $KHCO_3$, 3.722mg/L $EDTA.Na_2.2H_2O$) to eliminate erythrocytes, then all samples were washed, re-suspended in 10 ml sterile DMEM and filtered again to remove aggregated cells.

Eyes were enucleated, washed and all extraneous vascular and connective tissue was removed. The retina was then dissected microscopically in HBSS and retinas were physically disaggregated through a 40μM cell strainer and re-suspended in 200μl FACS buffer.

## Flow cytometric analysis

Cells were incubated with 24G2 cell supernatant for 20 minutes at 4°C before incubation with fluorochrome-conjugated monoclonal antibodies (BD Pharmingen, Oxford, UK) against cell surface markers including, CD4 (553051, 1/100), CD8 (553029, 1/100), CD11b (557657, 1/400), Ly6G (551461, 1/100), Ly6C (553104, 1/100) and CD45 (552848, 1/1000) at 4°C for 20

minutes. A streptavidin secondary antibody was added to all samples, (48-4317-82, eBioscience, San Diego, USA, 1/1000) then cell suspensions were acquired using a 3-laser BD LSR-II flow cytometer (BD Cytometry Systems, Oxford, UK). Analysis was performed using FlowJo software (Treestar, San Carlos, California, USA). Cell numbers were calculated by reference to a known cell–standard, as previously reported [14]. In brief, splenocytes at a series of known cell concentrations were acquired using a fixed and stable flow rate for 45 seconds. Based on total cell number acquired during this time, a standard curve was generated and used to interpolate cell concentrations of ocular infiltrating cells acquired at the same flow rate and time.

## Immunohistochemical analysis

12μm sections were cut from eyes snap frozen in OCT medium at -20°C, and mounted onto poly-L-lysine (Sigma, Poole, UK) coated glass slides. Sections were fixed in acetone for 10 minutes and endogenous peroxidases were blocked with 0.3% hydrogen peroxide and methanol for 30 minutes then washed in PBS. Blocking was achieved using normal rabbit serum (Vector Laboratories, Burlingame, California, USA) diluted in 2% bovine serum albumin (BSA) diluted in PBS (PBSA) for 30 minutes, followed by the addition of a rat anti-mouse primary antibody (MCA1388, AbDSerotec, Oxford, UK, 1/250), in 2% PBSA and left to incubate overnight at 4°C. A biotinylated rabbit anti-rat IgG secondary antibody (BA-4001, Vector, UK, 1/200), diluted in 0.1% PBSA was added to all sections for 30 minutes at room temperature then slides were coated with Avidin/Biotinylated enzyme complex (ABC kit, Vector Laboratories, Burlingame, California, USA) for 30 minutes. Sections were washed, coated with DAB reagent (DAKO, Denmark) for 2 minutes, and then immersed in haematoxylin stain. Slides were immediately washed and dehydrated by passage through 75% and 100% ethanol and Histoclear (National Diagnostics, Georgia, USA). Histomount (National Diagnostics, Georgia, USA) mounting media was used to affix coverslips and sections were examined under a light microscope. Clinical scoring was performed blind by an independent assessor based on cellular infiltrate and structural damage to the retina.

## Immunofluorescent staining

Staining for oxLDL was performed using a polyclonal rabbit anti-mouse antibody (ABIN1385598, Antibodies-online, Georgia USA, 1/100). 12-μm sections (as described above) were fixed using 4% PFA, then permeabilised and blocked using PBS supplemented with 0.25% Triton X-100, 1% BSA and 5% normal goat serum (Vector Laboratories, Burlingame, California, USA). Slides were washed in staining buffer (0.1% Triton X-100, 1% BSA in PBS) and incubated overnight at 4°C with 50μl staining buffer containing the oxLDL antibody plus a rat anti-mouse CD31 antibody directly conjugated with FITC (553372, BD Pharmingen, Oxford, UK, 1/100). Negative controls were treated with the latter only.

The following day, slides were washed and incubated for one hour with 50μl staining buffer containing goat anti-rabbit Alexa Fluor 568 (A-11011, Invitrogen, Paisley, UK, 1/200). Sections then received a final wash and were mounted using VECTASHIELD HardSet mounting media with DAPI (Vector Laboratories, Burlingame, California, USA). Immunofluorescence staining was examined using a confocal scanning laser imaging system fitted with krypton-argon lasers (TCS-SP2-AOBS; Leica microsystems, Wetzlar, Germany).

## SB-435495 plasma analysis

All plasma analysis was performed at GlaxoSmithKline. Briefly, SB-435495 was extracted from plasma (25 μL aliquot) using a protein precipitation method. Following vortexing and

centrifugation, an aliquot of the supernatant (100μL) was removed and diluted with 50μL of acetonitrile/10mM Ammonium Formate, pH3 (50/50, v/v) and mixed. Samples were quantitated for SB-435495 using a liquid chromatography mass spectrometry (UPLC-MS/MS) method. The LC-MS/MS system consisted of a Waters Acquity UPLC (Milford, MA) and an AB Sciex API 4000 triple quadrupole mass spectrometer (Framingham, MA) operating under Analyst 1.4.2 software (AB Sciex, Framingham, MA). The lower limit of quantification of SB-435495 was 1ng/ml and the upper limit of quantification was 1000ng/ml in the assay.

## Lp-PLA₂ assay

Quantification of Lp-PLA₂ enzyme activity in murine plasma was performed at GlaxoSmithKline via isolation of enzyme catalyzed release of [$^3$H-] acetate from the substrate 1-O-Hexadecyl-2-O-[$^3$H-] acetyl-sn-glycer-3-phophorylcholine ([$^3$H-]PAF obtained from Perkin Elmer, Waltham, MA. Product number: NET910250UC). Twenty microliters (20μL) of plasma was used for a single activity measurement using a 1 minute reaction time at 37°C. The Lp-PLA₂ enzyme reaction was quenched through chloroform:methanol (2:1 ratio) extraction of each individual reaction. Isolated activity (disintegrations per unit time (DPMs)) were extracted into the aqueous layer and converted to nanomoles of product through normalization to a [$^3$H-] PAF standard. Radioactivity (DPMs) was counted using a liquid scintillation counter (Beckman, Brea, CA). Inhibition of activity was gauged according to the activity level in the presence of inhibitor ("inhibited"), relative to blank or control plasma.

## Culture of bone marrow derived macrophages (BMDM)

Mice were sacrificed by cervical dislocation; the hind legs excised using aseptic technique, were placed in sterile DMEM and kept on ice. Following removal of the bone heads with a scalpel, bone marrow was flushed with un-supplemented DMEM. The marrow was then filtered through a 70μm cell strainer to remove debris. Cells were cultured in Teflon culture bags (provided by Dr. M. Munder, University of Heidelberg, Heidelberg, Germany) for eight days at 5–-10x10$^6$ cells per bag in 50ml of complete culture media supplemented with 50ng/ml macrophage colony stimulating factor and 5% Horse serum (Invitrogen).

## Stimulation of bone marrow derived macrophages

Macrophages were seeded at a concentration of 1 x10$^6$ cells/500μl per well in a 24 well plate. Cells were treated with either media alone, IL-4 (20ng/ml Peprotech, New Jersey, USA), prostaglandin-E₂ (PGE₂) (0.5 μg/ml Sigma-Aldrich, St Louis, USA), LPS (1–100ng/ml Sigma-Aldrich, St Louis, USA) or IFN-γ (0.5–50ng/ml Peprotech, New Jersey, USA) for 2, 4 or 24 hours as specified. Supernatants were removed and stored at -20°C for further assays.

## Nitrite Assay

50μl Griess reagent (Sigma-Aldrich, St Louis, USA) was added to BMDM supernatants (triplicate) and standards (9 point curve with 10,000nm top standard). Plates were read after five minutes, using a Spectramax-190 plate reader (Molecular Devices, California, USA) and Softmax-pro software, with absorbance wavelengths of 630nm and 540nm and a linear standard curve.

## Extracellular Lp-PLA₂ assay

Supernatants from BMDM samples, stimulated for 24 hours as described previously, were mixed with a 2-Thiol PAF substrate for one minute. In the presence of Lp-PLA₂ the substrate

was hydrolysed, producing a colorimetric change. Enzyme activity was calculated from the change in absorbance values read over a 15 minute period, using a Spectramax-190 plate reader and Softmax-pro software.

## Statistical analysis

Data are displayed using mean ± SEM. Analysis of continuous data with two variables was calculated using a T test. Those with 3 or more variables were calculated using a one or two way ANOVA as appropriate with a secondary Tukey test to determine the differences between treatment groups or Lp-PLA$_2$ genotype. Differences between groups were defined as significant at $P<0.05$.

## Results

To determine basal enzyme activity status of the Lp-PLA$_2$ KO, HET and WT mice, cardiac blood samples were processed for plasma analysis, which confirmed that Lp-PLA$_2$ activity was highest in WT animals, reduced in HETs and absent in Lp-PLA$_2$ KO mice (Fig 1A). Bone marrow derived macrophages (BMDM), stimulated with LPS (1ng/ml) or media alone for 2 or 4 hours, were used for RT-qPCR quantification of *Pla2g7* gene expression. The results confirmed *Pla2g7* gene expression was absent in Lp-PLA$_2$ KO mice, with the highest expression observed in Lp-PLA$_2$ WT mice (Fig 1B). To further determine expression and functionality of the secreted enzyme, an *in vitro* extracellular Lp-PLA$_2$ activity assay was performed (Cayman chemicals, Michigan, USA). Supernatants from media alone and LPS (1ng/ml) stimulated BMDM secreted detectable quantities of functional Lp-PLA$_2$, as indicated by the enzyme induced hydrolysis of a 2-Thio-PAF substrate and subsequent colorimetric change to the supernatant. Furthermore, when BMDM were pre-treated with the SB-435495 inhibitor at a range of doses before stimulation, the enzymatic reaction was absent or reduced (S1 Fig) indicating efficacy of the SB-435495 *in vitro*.

Prior to assessing the *in vivo* therapeutic efficacy of either Lp-PLA$_2$ deletion or inhibition, we wished to ascertain whether Lp-PLA$_2$ enzyme inhibition altered classical macrophage activation. ELISA estimation of IL-6 and MCP-1 was determined following LPS-stimulation of BMDM treated with a dose range of SB-435495. A trend towards a reduction in IL-6 protein expression was identified in macrophages treated with 10µM SB-435495, when compared to the untreated controls; however the inhibitor failed to significantly alter IL-6 and MCP-1 protein expression, (S2 Fig). To mimic physiological conditions the assay was further developed by spiking with endogenous oxLDL, as Lp-PLA$_2$ is transported *in vivo* on oxPL molecules within oxLDL. However the simultaneous addition of SB-435495 and exogenous oxLDL did not significantly alter IL-6 protein expression when compared to controls (Fig 2A). Given our observed sustained IL-6 response, we wished to confirm that IL-6 production was independent of Lp-PLA$_2$ and showed that LPS-stimulated BMDM from Lp-PLA$_2$ WT, HET and KO mice were equivalent and maintained an IL-6 dose response (Fig 2B).

qPCR analysis was utilised to examine expression of a number of characteristic phenotypic markers of macrophage activation status. Data showed no significant difference in IL-1β and IL-10 gene expression, as a signature of M1 and M2 macrophage activation respectively, in LPS stimulated BMDM from Lp-PLA$_2$ WT, HET and KO mice after both 2 and 4 hours in culture (Fig 3A and 3B). Quantification of the expression of Arginase-1 (Arg-1) and Nitric oxide synthase (iNOS or NOS2) was used as a further indicator of macrophage phenotype [32, 33]. Our data showed no significant difference in *Arg-1* expression from Lp-PLA$_2$ WT, HET or KO derived BMDM (Fig 3C). Further, a nitrite assay was used to determine whether Lp-PLA$_2$ deletion altered NOS2-dependent nitrite production as an indicator of M1 phenotype. Data
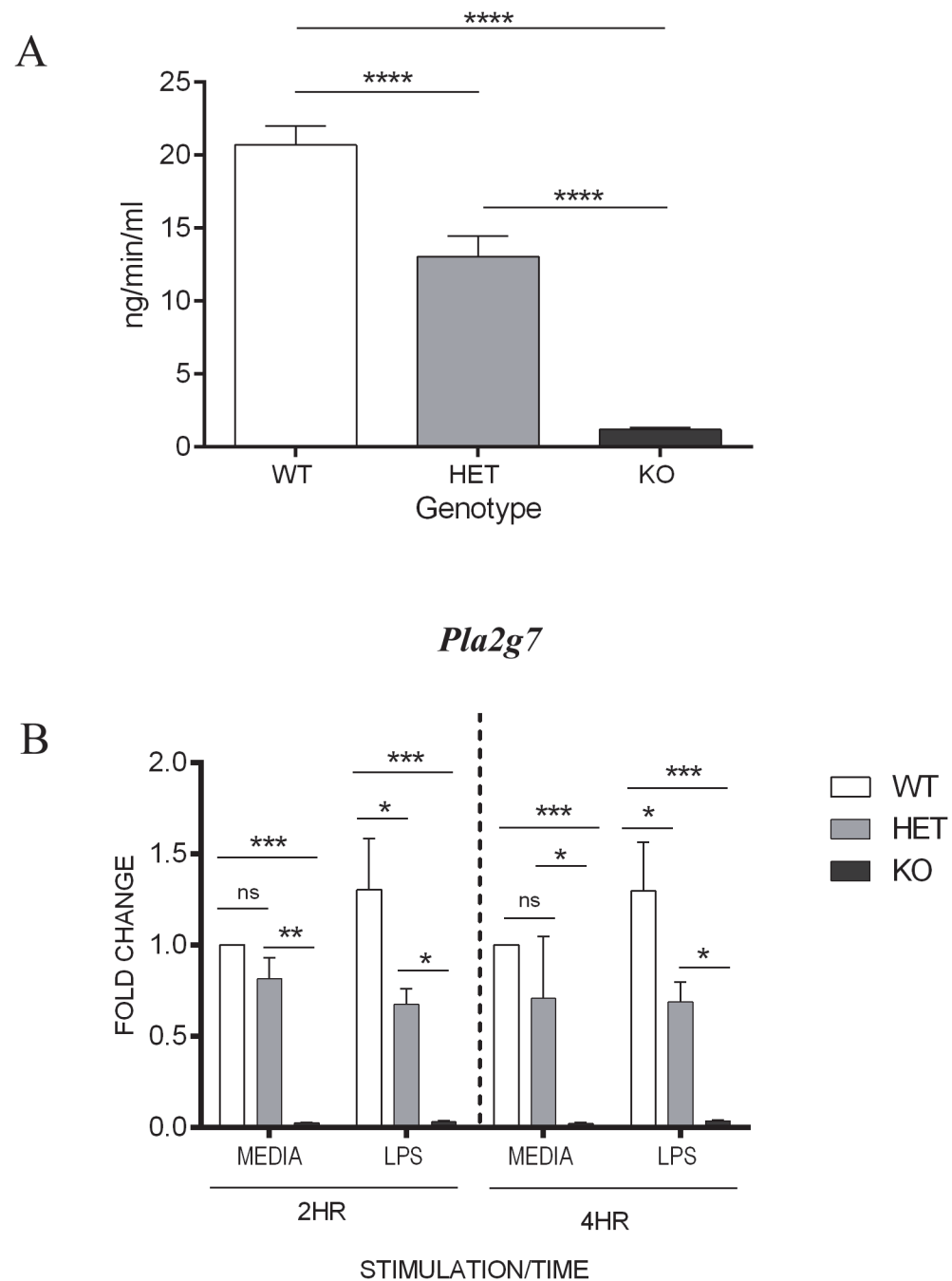
**Fig 1. Quantification of Lp-PLA2 enzyme activity and gene expression in murine plasmas and BMDM.**
**A)** Enzyme analysis of Lp-PLA$_2$ activity from murine cardiac blood samples (n = 15–17) **** $p < 0.001$. **B)**
RT-qPCR quantification of BMDM *Pla2g7* expression (n = 3). Lp-PLA$_2$ WT, HET and KO BMMO were
stimulated with LPS or media only for 2 or 4 hours, and gene expression analysed. *Pla2g7* mRNA expression
normalized by GAPDH. * $p < 0.05$ ** $p < 0.01$ *** $p < 0.005$

showed a dose-dependent, LPS mediated nitrite induction, which was independent of Lp-PLA$_2$
expression (Fig 3D). Nitrite production was also unchanged in LPS and IFNγ stimulated
BMDM from WT mice, cultured with doses of SB-435495 known to give optimal Lp-PLA$_2$ in-
hibition (Fig 3E).
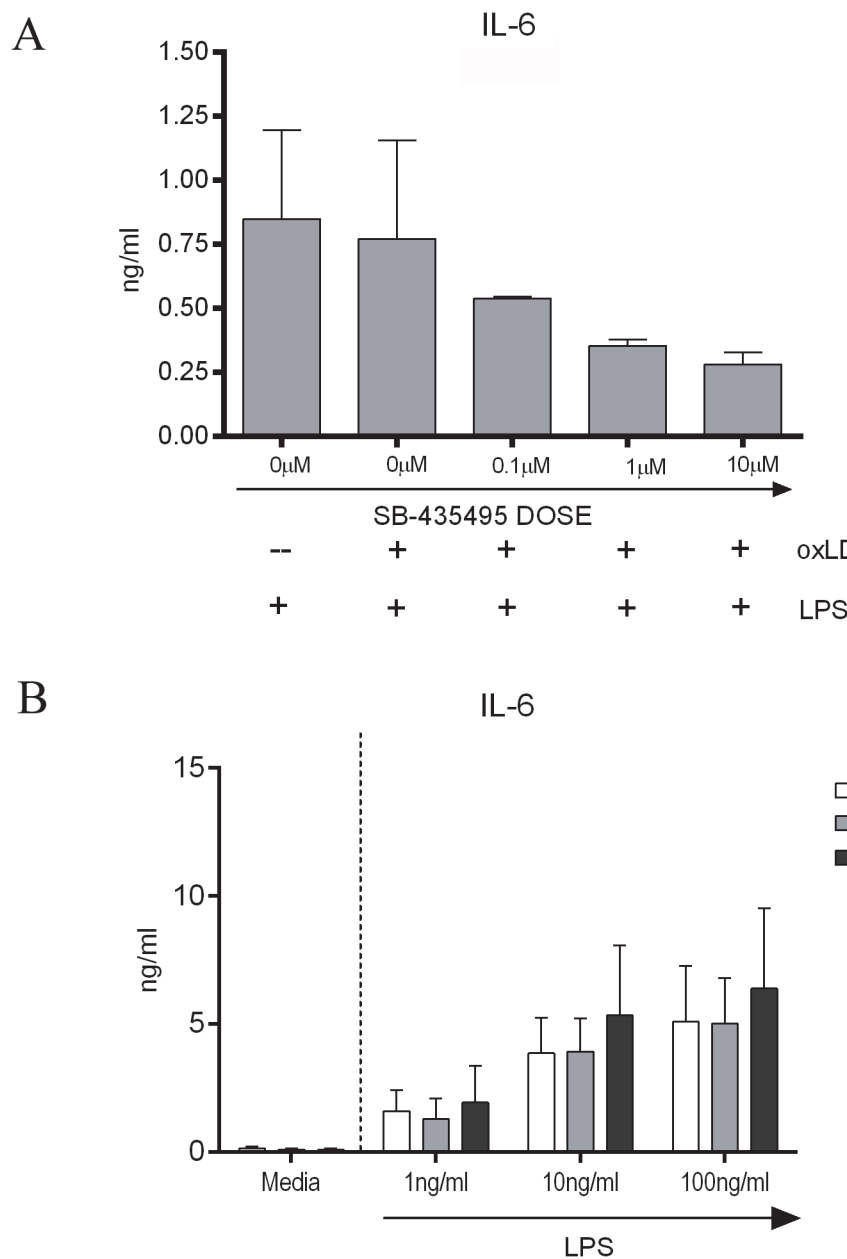
**Fig 2. Effect of Lp-PLA2 depletion on macrophage activation and phenotype on BMDM IL-6 protein expression.** Supernatants from BMDM cultured for 24 hours with SB-435495 treated oxLDL plus 1ng/ml LPS or media control were used to quantify IL-6 protein expression (n = 3). **A)** SB-435495 was not able to significantly alter IL-6 expression in LPS treated BMDM. IL-6 was undetected in media only controls. BMDM derived from Lp-PLA₂ WT, HET and KO mice were cultured with a titration of LPS. Supernatants were collected at 24 hours and used to quantify IL-6 protein expression by ELISA. **B)** There was no significant difference in IL-6 expression between Lp-PLA₂ WT, HET or KO BMDM.

doi:10.1371/journal.pone.0122093.g002

To further characterise the effect of Lp-PLA₂ deletion on macrophage phenotype, flow cytometry was used to quantify the expression of macrophage activation markers (CD68^{+} MHCII^{+} and CD40^{+} expression) in BMDM cultured from Lp-PLA₂ KO, HET and WT mice and stimulated with a panel of cytokines for 24 hours. The expression of MHCII and CD68 was unchanged when Lp-PLA₂ was deleted, however a significant reduction in CD40
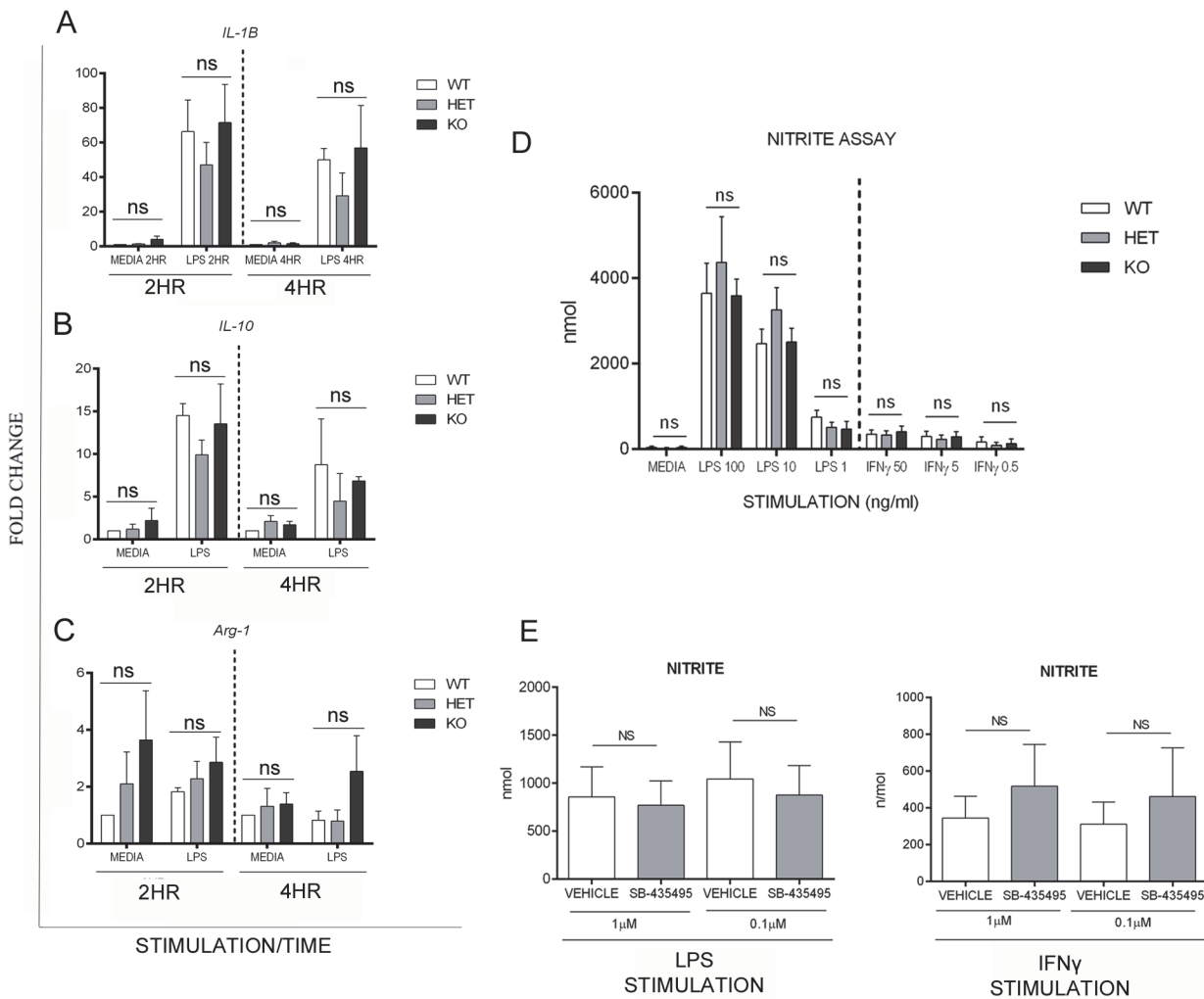
**Fig 3. Effect of Lp-PLA2 enzyme ablation on macrophage activation markers as an indicator of macrophage activation status.** Expression of IL-1β, IL-10 and Arginase-1 in Lp-PLA$_2$ WT, HET and KO mice by RT-qPCR. Data from BMDM, following 2 or 4 hour stimulation with LPS (1ng/ml) or media control **A)** IL-1β (n = 3–4) **B)** IL-10(n = 3) **C)** Arginase-1 (n = 3–4). **D)** A nitrite assay performed as described, using supernatants of BMDM from Lp-PLA$_2$ WT, HET and KO mice cultured in presence of LPS/IFNγ for 24 hours, showed no significant difference between genotypes (n = 9 from 5 mice). **E)** Data collected from nitrite assays using supernatants of BMDM treated with either LPS or IFNγ plus SB-435495 (1μM or 0.1μM) showed no significant difference between genotypes (n = 3) ****p<0.001

doi:10.1371/journal.pone.0122093.g003

expression was identified in LPS treated macrophages derived from Lp-PLA$_2$ HET and KO mice, when compared to WT control cells (Fig 4). Flow cytometric analysis of B and T cell marker expression in the thymus and spleen was also undertaken (CD45, CD3ε, B220, CD4, CD8, CD44, CD62L, CD69, CD25) which showed no significant difference between genotypes in naïve animals (S3 Fig).

Having ascertained the efficacy and functionality of SB-435495 *in vitro* we then wished to determine its effects *in vivo* using the well-established B10 RIII murine model of EAU. Following induction of EAU, mice were randomly allocated into treatment groups and received IP injections of SB-435495 or vehicle control at the doses and time points depicted in S4 Fig. Treatment continued until either day 14 (peak disease) or day 21 (disease resolution) when animals were sacrificed for analysis of retinal cellular infiltrate by flow cytometry and histology. An average Lp-PLA$_2$ inhibition of 50.2% and 54.3% (S5A Fig) was measured in plasma samples
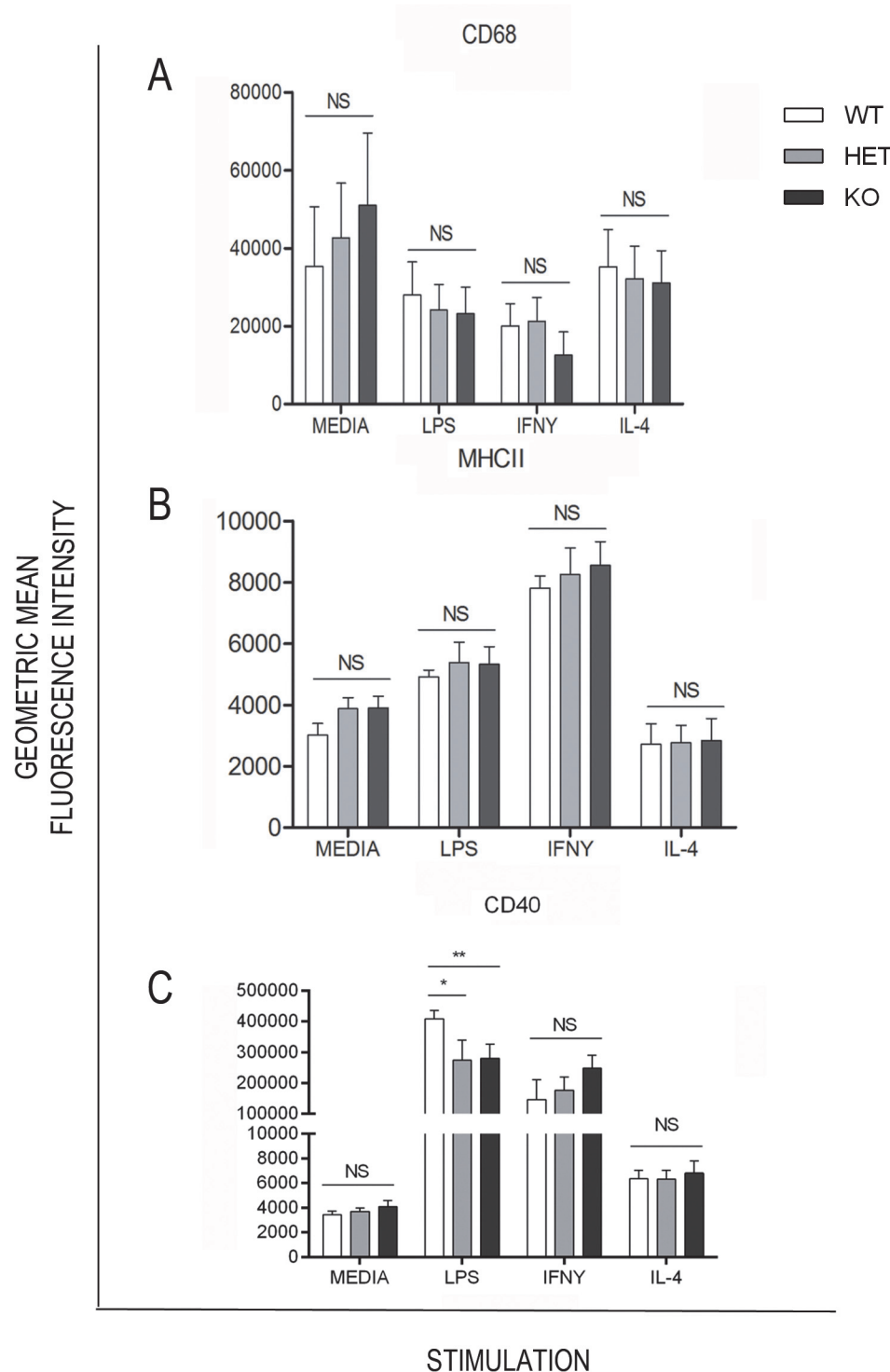
**Fig 4. Flow cytometric analysis of BMDM phenotype from cells cultured for 24 hours in the presence of a panel of cytokines.** Geometric mean fluorescence intensity values for **A)** intracellular CD68 expression (n = 4), **B)** cell surface MHCII expression (n = 3) and **C)** cell surface CD40 expression (n = 5) * $p < 0.05$ ** $p < 0.01$ *** $p < 0.005$

doi:10.1371/journal.pone.0122093.g004

taken at trough dosing (24h post previous dose) from B10 RIII mice treated once daily with either 20mg/kg or 35mg/kg SB-435495 respectively. Flow cytometry and histology data revealed that treatment of mice with this dose of SB-435495 did not reduce the number of infiltrating cells in the retinas of animals at day 14 or 21 post immunisation when compared to control animals (S5B Fig).

To achieve a more robust inhibition of Lp-PLA$_2$ activity, mice were treated twice daily from day 5 post immunisation, with SB-435495 in the hope of maintaining more consistent enzyme inhibition. Mice were given IP injections of 30mg/kg of SB-435495, every 12 hours (S4 Fig). Analysis of plasma samples taken from mice at day 14 post immunisation showed 89.9% inhibition of Lp-PLA$_2$ at trough dosing (12 hours post previous dose) (S6A Fig). In spite of this reduction in enzyme activity, there were equivalent numbers of CD45$^+$ infiltrating leukocytes in the retina of these mice by flow cytometry (Fig 5A) and histology (Fig 5B). Furthermore, clinical scoring of TEFI images showed no change to longitudinal disease progression and no significant difference in EAU between treatment groups (Fig 5C).

As the data suggested partial Lp-PLA$_2$ inhibition was insufficient to abrogate retinal leukocyte infiltration, we then wished to assess the effect of permanent and complete deletion of Lp-PLA$_2$ in EAU. As such, C57BL/6 Lp-PLA$_2$ KO mice were utilised for subsequent experiments, with HET and WT littermates as controls. Mice were sacrificed at day 26 (peak disease) for analysis by flow cytometry and histology. However, in spite of the systemic deletion of Lp-PLA$_2$, a comparable number of cells (CD45$^+$, CD11b$^+$, CD4$^+$, CD8$^+$) were found to infiltrate the retina during EAU in Lp-PLA$_2$ KO mice and HET/WT littermate controls (Fig 6).

Oxidation of LDL is an important step in the onset and progression of atherosclerosis. Oxidation of the lipoprotein molecule prevents binding to the LDL receptors and infers an increased affinity for macrophage scavenger receptors such as CD36 and LOX-1[34]. This is turn leads to reduced macrophage migration and the formation of lipid-laden foam cells, which are key features of an atherosclerotic plaque. However, less is known about the role of oxLDL in EAU and as such immunohistochemical staining of the Lp-PLA$_2$ substrate was used to characterise its availability and distribution in both a healthy and uveitic eye. Data revealed that oxLDL was not detected in the naïve retina (Fig 7A), but in the uveitic retina appeared to co-localise to the vasculature and outer plexiform layer (Fig 7B).

## Discussion

We have successfully shown that SB-435495 is an effective, reversible inhibitor of Lp-PLA$_2$ both in BMDM *in vitro* and in an *in vivo* murine model of EAU. A small amount of platelet activating factor acetyl hydrolase (PAF-AH) activity was detected in the serum of Lp-PLA$_2$ KO mice (Fig 1A), however this is not thought to be Lp-PLA$_2$ as it is not inhibited with SB-435495 at concentrations >20uM which are 200% effective on the isolated enzyme [29]. Significant Lp-PLA$_2$ inhibition with SB-435495 was not able to significantly alter the cytokine profile of BMDM *in vitro*, but cells treated with the inhibitor did show a trend towards a dose dependent reduction in the expression of IL-6. Furthermore, *in vivo*, Lp-PLA$_2$ deletion or inhibition had no effect on EAU induction or onset.

Lp-PLA$_2$ is so called because in humans 80% of the circulating enzyme is carried on apolipoprotein-B100 moieties on low density lipoprotein (LDL) molecules [35]. The remaining 20% is carried on high density lipoprotein (HDL) and very low density lipoprotein (VLDL) molecules, while in mice the ratios are reversed, due to minimal expression of LDL in this species. Increased Lp-PLA$_2$ mass and activity has been identified as a biomarker for coronary heart disease, and is found in patients with high cardiovascular risk factors [24]. It is also known to be associated with major adverse events in patients with coronary artery disease in a CRP
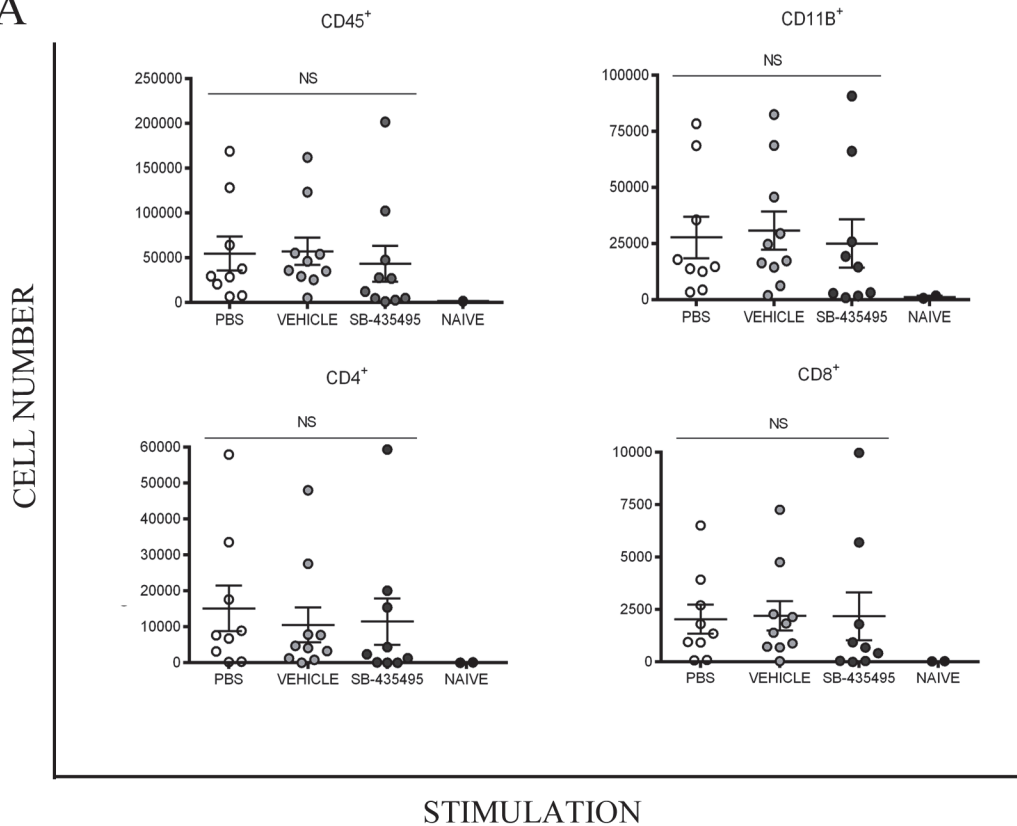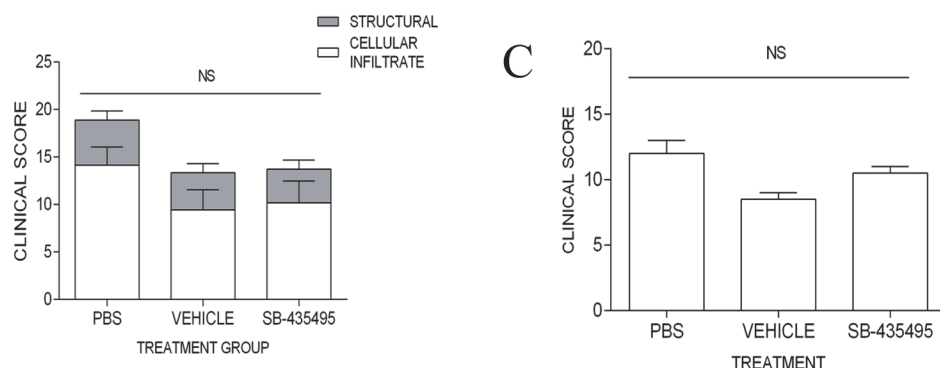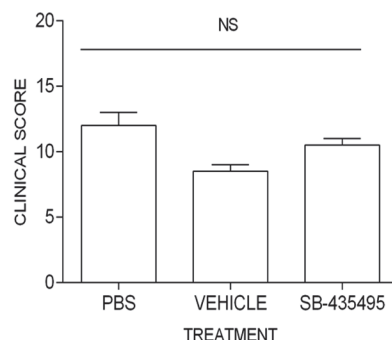
**Fig 5. Quantification of retinal cellular infiltrate and onset of clinical disease in a murine model of EAU; effective of SB-435454. A)** Flow cytometry data showing CD45+, CD11b+, CD4+ and CD8+ cellular infiltrate in retinal digests from animals at day 14 post immunisation, treated twice daily with either SB-435495 or controls (n = 9–10 eyes). **B)** Histological staining scores from 12μm ocular sections taken from eyes enucleated at day 14 post immunisation, stained for CD45+ (DAB/haematoxylin) (n = 9–10 eyes). **C)** TEFI clinical score, day 13 post immunisation, (average scores provided by two independent assessors from two identical repeat experiments. n = 18–20).

doi:10.1371/journal.pone.0122093.g005
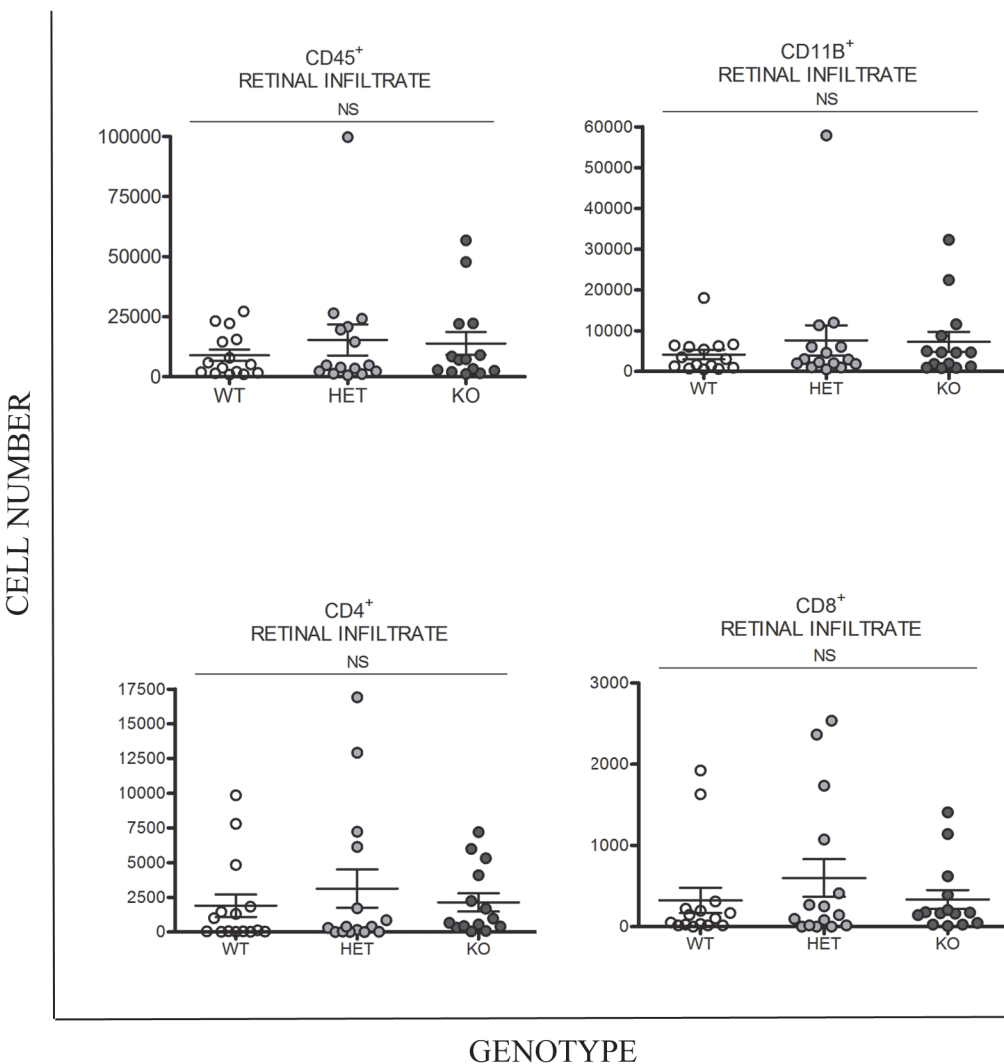
**Fig 6. Quantification of retinal cellular infiltrate at day 26 post immunisation in a C57BL/6 murine model of EAU carrying Lp-PLA2 WT, heterozygous and homozygous gene-deletion genotypes.** Flow cytometry data showing CD45$^+$, CD11b$^+$, CD4$^+$ and CD8$^+$ cellular infiltrate in retinal digests from Lp-PLA$_2$ KO, HET, WT animals with EAU at day 26 post immunisation. (n = 14–15 eyes).

doi:10.1371/journal.pone.0122093.g006

independent manner [35]. Lp-PLA$_2$ is considered a key enzyme in vascular inflammation, due to its ability to catalyse the hydrolysis of oxPL on oxLDL molecules in the intima of blood vessels resulting in the production of ox-NEFA and LPC, which are cytotoxic and have a potent effect on many different cell types.

As such, the notion of Lp-PLA$_2$ suppression as a therapeutic target has received much interest in recent years. A porcine model, using streptozotocin treatment and a high fat, high cholesterol diet was used to induce diabetes and accelerate subsequent onset of atherosclerosis. Treatment with the Lp-PLA$_2$ inhibitor, Darapladib, resulted in a reduction of Lp-PLA$_2$ activity and atherosclerotic plaque size, IL-6 expression and systemic hCRP. Whether such response would be evident in a T cell driven autoimmune model, where both macrophage activation and inflammatory vasculopathy are evident, was the rationale for the current work.

oxLDL molecules have been shown not only to carry the enzyme, but also to up-regulate Lp-PLA$_2$ expression in the human THP-1 monocyte cell line [36] and data show that when
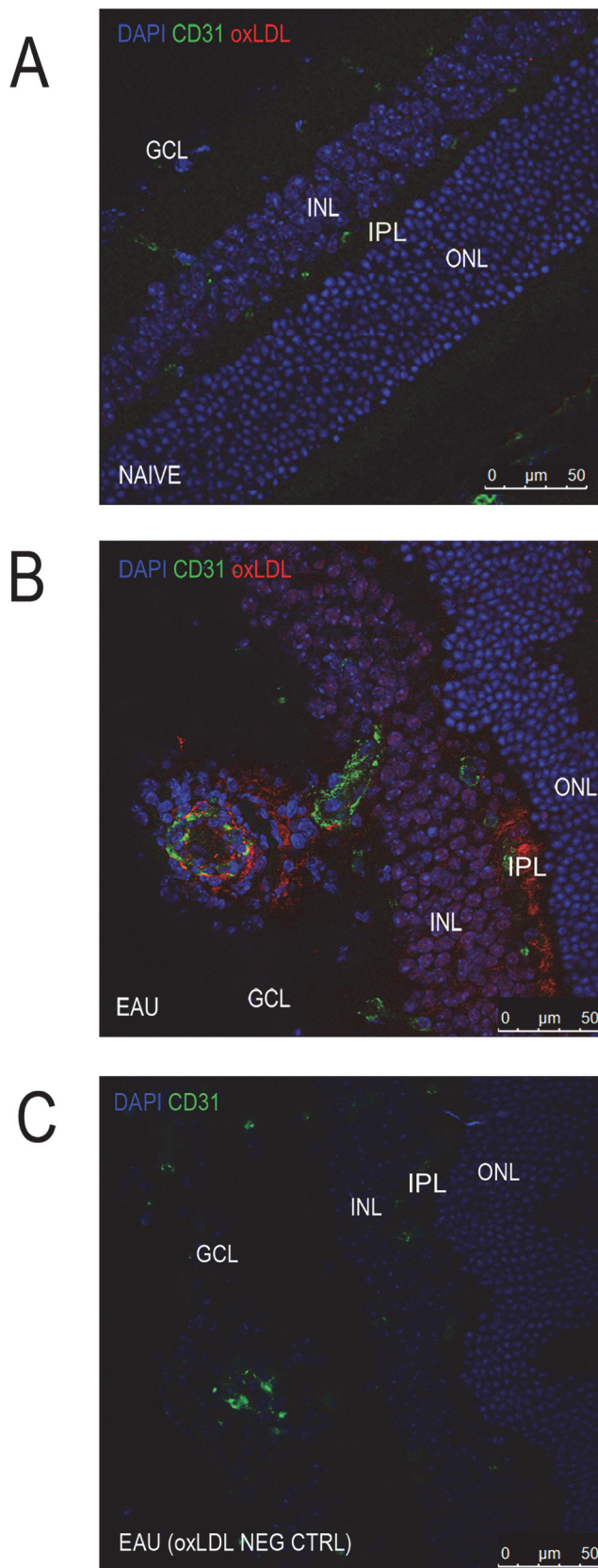
**Fig 7. Ocular oxLDL in naive and uveitic mice.** Immunofluorescence staining of DAPI (blue) oxLDL (red) and CD31 (green) using 12μm ocular sections from **A)** naïve mice or **B-C)** those immunised for EAU (sequential slides). Ganglion cell layer (GCL), inner nuclear layer (INL), inner plexiform layer (IPL), outer nuclear layer (ONL).

oxLDL is treated with SB-435495, Lp-PLA₂ activity is reduced [36]. Furthermore, macrophage expression of Lp-PLA₂ is increased by TLR4 ligation with LPS, due to a P38 MAPK mediated transcriptional up-regulation [37], suggesting that the enzyme is likely to be highly expressed during inflammation. As such, we hypothesised that by suppressing Lp-PLA₂ enzyme activity it may be possible to alter macrophage phenotype and subvert the subsequent macrophage-mediated tissue damage that occurs in EAU. To this end, both LPS and oxLDL were used to stimulate BMDM, and we did note a trend towards a dose response of SB-435495 in IL-6 expression (Fig 2A).

MCP-1 expression plays an important role in myeloid cell migration in uveitis and the products of oxLDL breakdown, LPC and NEFA, up-regulate macrophage MCP-1 production, a response we hoped to attenuate by depleting Lp-PLA₂. However, SB-435495 failed to reduce MCP-1 expression from LPS stimulated BMDM (S2B Fig). oxLDL itself is also capable of inducing MCP-1 expression in macrophages [38] and we therefore postulate the possibility that an equilibrium exists between the influence of oxLDL and the associated hydrolytic bi-products on myeloid cells *in vitro*. Lp-PLA₂ depletion may cause oxLDL to accumulate, with the potential to induce MCP-1 production, hence negating any beneficial effects of SB-43545. oxLDL also induces myeloid IL-1β production [39] and hence could explain why Lp-PLA₂ HET BMDM, with intermediate enzyme activity, show the lowest gene expression of *IL-1β* see by qPCR (Fig 3A). In addition to the effect on MCP-1 and IL-1β expression, recent publications have identified a link between oxLDL, and differentiation of cells of the CD4+ TH17 lineage. Using an *in vitro* co-culture of T cells and dendritic cells treated with TGF-β and oxLDL, an up-regulation of TH17 cell differentiation has been identified, which was absent in samples treated with native LDL or an oxLDL depletion antibody [40]. As such, it is possible that both the substrate and bi-products of the Lp-PLA₂ reaction have the potential to exacerbate autoimmune disease.

Our data show no significant change to *in vitro Arg-1* expression in response to altered Lp-PLA₂ activity (Fig 3C) and similarly, BMDM expression of *IL-10*, an anti-inflammatory cytokine, was unchanged in KO mice when compared to WT control cells (Fig 3B). Furthermore, in BMDM derived from Lp-PLA₂ WT, HET and KO mice, there was a dose-dependent LPS mediated nitrite production, but this remained independent of Lp-PLA₂ activity (Fig 3D). As such, these data infer that depletion of the Lp-PLA₂ enzyme does not significantly alter macrophage phenotype.

The activity of Lp-PLA₂ is regulated to an extent by the degree of HDL and LDL binding, which delivers either anti or pro inflammatory/atherosclerotic behaviour respectively as observed in man. Unlike LDL, HDL acts to remove cholesterol from lipid laden foam cells in the vessel intima and acts as an anti-oxidant, reducing the ability of LDL to become oxidised by removal of lipid hydroperoxidases [41]. The behaviour and phenotype of HDL and LDL carrier molecules can be altered in chronic conditions such as type II diabetes, where increased small dense LDL (sdLDL) molecules afford greater affinity for Lp-PLA₂ [42]. Similarly, diabetic patients have been shown to have HDL molecules with reduced anti-oxidant behaviour owing to an imbalance of lipid/protein and apoA-I/apoA-II ratios [42]. These lipid modifications contribute to the onset of atherosclerosis, but are unlikely to be observed in the context of subacute T cell driven tissue inflammation such as that seen uveitis.

Whilst EAU is comparable in many respects to both atherosclerosis and diabetic macular oedema, demonstrating macrophage and TH17$^+$ cell mediated vascular pathology, EAU does not share the same underlying dyslipidaemic traits and therefore it is possible this is why we did not observe an effect in EAU despite the involvement of inflammation, macrophage infiltration and vessel inflammation in this model.

In the normal retina there appears to be limited expression of oxLDL (Fig 7A), which increases when disease is fulminant (Fig 7B). We had predicted that activation, phenotype and migration of circulating myeloid cells might be altered by systemic Lp-PLA$_2$ depletion and hence the ocular availability of the substrate would be unimportant. However quantification of retinal leukocyte infiltration during peak disease, by both flow cytometry and histology revealed no difference between Lp-PLA$_2$ depleted samples and controls, indicating that the control of migration of cells into the tissue, driven by antigen specific T cell activation, was independent of Lp-PLA$_2$ activity.

Interestingly, and in accordance with our work, recent publications have stated that in spite of promising preliminary findings, Darapladib treatment and associated Lp-PLA$_2$ reduction failed to significantly reduce the incidence of myocardial infarction, stroke and cardiovascular death in a cohort of patients with coronary heart disease, when compared to a placebo treated control group following an extensive randomised, multicentre phase III clinical trial, [43]. Similarly, whilst we were able to show a clear reduction in systemic Lp-PLA$_2$, which resulted in some alteration to macrophage cytokine profiles, our data show that manipulation of Lp-PLA$_2$ does not alter the onset or progression of EAU. It seems therefore that the acute inflammatory pathways involved in EAU onset proceed independently of Lp-PLA$_2$ mediated mechanisms.

## Supporting Information

**S1 Fig. Expression and functionality of secreted Lp-PLA$_2$.** Supernatants from **A)** media alone and **B)** LPS (1ng/ml) stimulated BMDM were found to secrete detectable quantities of functional Lp-PLA$_2$, as indicated by a colorimetric change to the supernatant as a result of hydrolysis of a labelled 2-Thio PAF substrate. This response was abrogated in the presence of SB-435495 treatment.
(TIF)

**S2 Fig. Effect of Lp-PLA$_2$ depletion on macrophage activation and phenotype.** Supernatants from BMDM pre-treated with a dose titration of SB-435495 plus 1ng/ml LPS were used to quantify expression of IL-6 and MCP-1 by ELISA. n = 3 p>0.05. SB-435495 did not significantly reduce either **A)** IL-6 or **B)** MCP-1 protein expression from LPS treated BMDM (n = 3)
(TIF)

**S3 Fig. Immune phenotype in naïve Lp-PLA$_2$ WT, HET and KO mice.** Quantification of B and T cell populations from **A)** the thymus and **B)** the spleen using geometric mean fluorescence intensity (GMFI). GMFI quantification of CD4$^+$ T cell activation markers from **C)** thymocytes and **D)** splenocytes and CD8$^+$ T cell activation markers from **E)** thymocytes and **F)** splenocytes.
(TIF)

**S4 Fig. Dosing regimen for *in vivo* EAU experiments using SB-435495.** Mice were immunised and randomly allocated to a treatment group. Each mouse was given a standardised daily or twice daily volume of SB-435495 by i.p injection and the dose calculated based on the weight of the animal.
(TIF)

**S5 Fig. Daily treatment with 20mg/kg or 35mg/kg SB-435495 did not significantly reduce the number of cells infiltrating the retina. A)** Percent inhibition calculated from murine plasma, taken at time of sacrifice (n = 3) **B)** Quantification of cells infiltrating the retina at day 14 and 21 post immunisation (n = 3) ** $p < 0.01$
(TIF)

**S6 Fig. *Twice daily* treatment with 30mg/kg SB-435495 significantly reduced Lp-PLA₂ activity in murine plasma. A)** % Lp-PLA₂ inhibition and **B)** Lp-PLA₂ enzyme activity calculated from murine plasma, taken at time of sacrifice (n = 14–15). *** $p < 0.005$ **** $p < 0.001$
(TIF)

## Acknowledgments

## Author Contributions

Conceived and designed the experiments: GLC JB DAC PA DG MB LBN ADD. Performed the experiments: GLC JB DAC DG MB. Analyzed the data: GLC JB DAC PA DG MB LBN ADD. Contributed reagents/materials/analysis tools: PA DG MB. Wrote the paper: GLC JB DAC PA DG MB LBN ADD.

## References

1. Selmi C. Diagnosis and classification of autoimmune uveitis. Autoimmunity reviews. 2014; 13(4):591–4. doi: 10.1016/j.autrev.2014.01.006 PMID: 24424168

2. (WHO) WHO. Global data on visual impairments 2010 [cited 2014 July 01].

3. Yeo TK, Ho SL, Lim WK, Teoh SC. Causes of Visual Loss Associated with Uveitis in a Singapore Tertiary Eye Center. Ocular Immunology & Inflammation. 2013; 21(4):264–9.

4. Shewitz-Bowers L, Lee R.W.J., Dick A.D. Immune mechanisms of intraocular inflammation. Expert Reviews. 2010; 5(1):43–58.

5. Forrester JV, Liversidge J, Dick A, McMenamin P, Kuppner M, Crane I, et al. What determines the site of inflammation in uveitis and chorioretinitis? Eye. 1997; 11(2):162–6.

6. Forrester JV, Klaska IP, Yu T, Kuffova L. Uveitis in mouse and man. International reviews of immunology. 2013; 32(1):76–96. doi: 10.3109/08830185.2012.747524 PMID: 23360160

7. Kerr EC, Copland DA, Dick AD, Nicholson LB. The dynamics of leukocyte infiltration in experimental autoimmune uveoretinitis. Progress in Retinal and Eye Research. 2008; 27(5):527–35. doi: 10.1016/j.preteyeres.2008.07.001 PMID: 18723108

8. Copland DA, Wertheim MS, Armitage WJ, Nicholson LB, Raveney BJ, Dick AD. The clinical time-course of experimental autoimmune uveoretinitis using topical endoscopic fundal imaging with histologic and cellular infiltrate correlation. Investigative ophthalmology & visual science. 2008; 49(12):5458–65.

9. Copland DA, Calder CJ, Raveney BJ, Nicholson LB, Phillips J, Cherwinski H, et al. Monoclonal antibody-mediated CD200 receptor signaling suppresses macrophage activation and tissue damage in experimental autoimmune uveoretinitis. The American journal of pathology. 2007; 171(2):580–8. PMID: 17600119

10. Forrester JV, Huitinga I, Lumsden L, Dijkstra CD. Marrow-derived activated macrophages are required during the effector phase of experimental autoimmune uveoretinitis in rats. Current eye research. 1998; 17(4):426–37. PMID: 9561835

11. Calder CJ, Nicholson LB, Dick AD. A selective role for the TNF p55 receptor in autocrine signaling following IFN-γ stimulation in experimental autoimmune uveoretinitis. The Journal of Immunology. 2005; 175(10):6286–93. PMID: 16272279

12.  Dick AD, McMenamin PG, Körner H, Scallon BJ, Ghrayeb J, Forrester JV, et al. Inhibition of tumor necrosis factor activity minimizes target organ damage in experimental autoimmune uveoretinitis despite quantitatively normal activated T cell traffic to the retina. European journal of immunology. 1996; 26 (5):1018–25. PMID: 8647162

13.  Xu H, Forrester JV, Liversidge J, Crane IJ. Leukocyte trafficking in experimental autoimmune uveitis: breakdown of blood–retinal barrier and upregulation of cellular adhesion molecules. Investigative ophthalmology & visual science. 2003; 44(1):226–34.

14.  Kerr EC, Raveney BJ, Copland DA, Dick AD, Nicholson LB. Analysis of retinal cellular infiltrate in experimental autoimmune uveoretinitis reveals multiple regulatory cell populations. Journal of autoimmunity. 2008; 31(4):354–61. doi: 10.1016/j.jaut.2008.08.006 PMID: 18838247

15.  Raveney BJ, Copland DA, Calder CJ, Dick AD, Nicholson LB. TNFR1 signalling is a critical checkpoint for developing macrophages that control of T–cell proliferation. Immunology. 2010; 131(3):340–9. doi: 10.1111/j.1365-2567.2010.03305.x PMID: 20518824

16.  Raveney BJ, Copland DA, Dick AD, Nicholson LB. TNFR1-dependent regulation of myeloid cell function in experimental autoimmune uveoretinitis. The Journal of Immunology. 2009; 183(4):2321–9. doi: 10.4049/jimmunol.0901340 PMID: 19635911

17.  Lee R, Dick A. Current concepts and future directions in the pathogenesis and treatment of non-infectious intraocular inflammation. Eye. 2011; 26(1):17–28. doi: 10.1038/eye.2011.255 PMID: 21960067

18.  Lee RW, Nicholson LB, Sen HN, Chan C-C, Wei L, Nussenblatt RB, et al., editors. Autoimmune and autoinflammatory mechanisms in uveitis. Seminars in immunopathology; 2014: Springer.

19.  Six DA, Dennis EA. The expanding superfamily of phospholipase A2 enzymes: classification and characterization. Biochimica et Biophysica Acta (BBA)-Molecular and Cell Biology of Lipids. 2000; 1488(1–2):1–19.

20.  Schmitz G, Ruebsaamen K. Metabolism and atherogenic disease association of lysophosphatidylcholine. Atherosclerosis. 2010; 208(1):10–8. doi: 10.1016/j.atherosclerosis.2009.05.029 PMID: 19570538

21.  Arai H. Platelet activating factor acetylhydrolase (PAF-AH). Prostaglandins and other lipid mediators. 2002:68–9 83–94.

22.  McIntyre TM, Prescott SM, Stafforini DM. The emerging roles of PAF acetylhydrolase. Journal of lipid research. 2009; 50(Supplement):S255–S9.

23.  Adamson P, Lee D. Use of LP-PLA2 Inhibitors in the Treatment and Prevention of Eye Diseases. US Patent 20,130,267,544; 2013.

24.  Collaboration L-PS. Lipoprotein-associated phospholipase A2 and risk of coronary disease, stroke, and mortality: collaborative analysis of 32 prospective studies. Lancet. 2010; 375(9725):1536. doi: 10.1016/S0140-6736(10)60319-4 PMID: 20435228

25.  Blackie JA, Bloomer JC, Brown MJ, Cheng H-Y, Hammond B, Hickey D, et al. The identification of clinical candidate SB-480848: a potent inhibitor of lipoprotein-associated phospholipase A₂. Bioorganic & medicinal chemistry letters. 2003; 13(6):1067–70.

26.  Wilensky RL, Shi Y, Mohler ER, Hamamdzic D, Burgert ME, Li J, et al. Inhibition of lipoprotein-associated phospholipase A2 reduces complex coronary atherosclerotic plaque development. Nature medicine. 2008; 14(10):1059–66. doi: 10.1038/nm.1870 PMID: 18806801

27.  Serruys PW, García-García HM, Buszman P, Erne P, Verheye S, Aschermann M, et al. Effects of the direct lipoprotein-associated phospholipase A2 inhibitor darapladib on human coronary atherosclerotic plaque. Circulation. 2008; 118(11):1172–82. doi: 10.1161/CIRCULATIONAHA.108.771899 PMID: 18765397

28.  Wang W, Zhang J, Wu W, Li J, Ma Y, Chen W, et al. Inhibition of Lipoprotein-Associated Phospholipase A2 Ameliorates Inflammation and Decreases Atherosclerotic Plaque Formation in ApoE-Deficient Mice. PloS one. 2011; 6(8):e23425. doi: 10.1371/journal.pone.0023425 PMID: 21909350

29.  Jiang Z, Fehrenbach ML, Ravaioli G, Kokalari B, Redai IG, Sheardown SA, et al. The effect of lipoprotein-associated phospholipase A2 deficiency on pulmonary allergic responses in aspergillus fumigatus sensitized mice. Respiratory research. 2012; 13(1):100.

30.  Paques M, Guyomard JL, Simonutti M, Roux MJ, Picaud S, LeGargasson JF, et al. Panretinal, high-resolution color photography of the mouse fundus. Investigative Ophthalmology & Visual Science. 2007; 48(6):2769–74.

31.  Xu H, Koch P, Chen M, Lau A, Reid DM, Forrester JV. A clinical grading system for retinal inflammation in the chronic model of experimental autoimmune uveoretinitis using digital fundus images. Exp Eye Res. 2008; 87(4):319–26. doi: 10.1016/j.exer.2008.06.012 PMID: 18634784

32.  Mosser DM, Edwards JP. Exploring the full spectrum of macrophage activation. Nature Reviews Immunology. 2008; 8(12):958–69. doi: 10.1038/nri2448 PMID: 19029990

33. Gordon S. Alternative activation of macrophages. Nature Reviews Immunology. 2003; 3(1):23–35. PMID: 12511873

34. Shoji T, Nishizawa Y, Fukumoto M, Shimamura K, Kimura J, Kanda H, et al. Inverse relationship between circulating oxidized low density lipoprotein (oxLDL) and anti-oxLDL antibody levels in healthy subjects. Atherosclerosis. 2000; 148(1):171–7. PMID: 10580183

35. Brilakis ES, McConnell JP, Lennon RJ, Elesber AA, Meyer JG, Berger PB. Association of lipoprotein-associated phospholipase A2 levels with coronary artery disease risk factors, angiographic coronary artery disease, and major adverse events at follow-up. European heart journal. 2005; 26(2):137–44. PMID: 15618069

36. Wang WY, Li J, Yang D, Xu W, Zha R, Wang Y. OxLDL stimulates lipoprotein-associated phospholipase A2 expression in THP-1 monocytes via PI3K and p38 MAPK pathways. Cardiovascular research. 2010; 85(4):845–52. doi: 10.1093/cvr/cvp367 PMID: 19910444

37. Zalewski A, Macphee C. Role of lipoprotein-associated phospholipase A2 in atherosclerosis. Arteriosclerosis, thrombosis, and vascular biology. 2005; 25(5):923–31. PMID: 15731492

38. Lim H, Kim YU, Sun H, Lee JH, Reynolds JM, Hanabuchi S, et al. Proatherogenic conditions promote autoimmune T helper 17 cell responses in vivo. Immunity. 2014; 40(1):153–65. doi: 10.1016/j.immuni.2013.11.021 PMID: 24412615

39. Liu W, Yin Y, Zhou Z, He M, Dai Y. OxLDL-induced IL-1beta secretion promoting foam cells formation was mainly via CD36 mediated ROS production leading to NLRP3 inflammasome activation. Inflammation Research. 2014; 63(1):33–43. PMID: 24121974

40. Chung Y, Lim H, Kim YU, Sun H, Hanabuchi S, Teng B. Proatherogenic conditions promote autoimmune Th17 responses in vivo (P4136). The Journal of Immunology. 2013; 190:191.14.

41. Kotosai M, Shimada S, Kanda M, Matsuda N, Sekido K, Shimizu Y, et al. Plasma HDL reduces nonesterified fatty acid hydroperoxides originating from oxidized LDL: a mechanism for its antioxidant ability. Lipids. 2013; 48(6):569–78. doi: 10.1007/s11745-013-3779-1 PMID: 23494578

42. Sánchez-Quesada JL, Vinagre I, De Juan-Franco E, Sánchez-Hernández J, Bonet-Marques R, Blanco-Vaca F, et al. Impact of the LDL subfraction phenotype on Lp-PLA2 distribution, LDL modification and HDL composition in type 2 diabetes. Cardiovasc Diabetol. 2013; 12:112. doi: 10.1186/1475-2840-12-112 PMID: 23915379

43. White HD, Held C, Stewart R, Tarka E, Brown R, Davies RY, et al. Darapladib for preventing ischemic events in stable coronary heart disease. The New England journal of medicine. 2014; 370(18):1702. doi: 10.1056/NEJMoa1315878 PMID: 24678955